polymers

MDPI

Article

Design and Construction of an Azo-Functionalized POP for Reversibly Stimuli-Responsive CO_2 Adsorption

Rongrong Yuan *, Meiyu Zhang and Hao Sun

Department of Materials Science and Engineering, Jilin Jianzhu University, Changchun 130118, China
* Correspondence: yuanrongrong@jlju.edu.cn

Abstract: A porous azo-functionalized organic polymer (JJU-2) was designed and prepared via oxidative coupling polymerization promoted by $FeCl_3$. JJU-2 exhibited reversibly stimuli-responsive CO_2 adsorption properties as a result of the trans/cis isomerization of the polymer's azo-functionalized skeleton. Under UV irradiation and heat treatment, this porous material displayed various porous structures and CO_2 adsorption properties. The initial Brunauer-Emmett-Teller (BET) surface area of JJU-1 is 888 $m^2\ g^{-1}$. After UV irradiation, the BET surface area decreases to 864 $m^2\ g^{-1}$, along with the decrease of micropores around 0.50 nm and 1.27 nm during the trans-to-cis isomerization process. In addition, CO_2 sorption isotherms demonstrate an 8%t decrease, and the calculated Qst of CO_2 has decreased from 29.0 kJ mol^{-1} to 26.5 kJ mol^{-1} due to the trans to cis conversion of the azobenzene side group. It is noteworthy that JJU-2′s CO_2 uptakes are nearly constant over three cycles of alternating external stimuli. Therefore, this azo-functionalized porous material was a potential carbon capture material that was responsive to stimuli.

Keywords: porous organic polymer; azobenzene; trans/cis isomerization; CO_2 sorption

check for updates

Citation: Yuan, R.; Zhang, M.; Sun, H. Design and Construction of an Azo-Functionalized POP for Reversibly Stimuli-Responsive CO_2 Adsorption. *Polymers* **2023**, *15*, 1709. https://doi.org/10.3390/polym15071709

Academic Editor: Youliang Cheng

Received: 16 January 2023
Revised: 27 March 2023
Accepted: 27 March 2023
Published: 29 March 2023

1. Introduction

Modern industrial-era greenhouse gas emissions have a significant impact on global warming and environmental change. Carbon dioxide (CO_2) is regarded as one of the most important greenhouse gases, resulting in an increased focus on reducing or capturing CO_2. Unfortunately, the concentration of CO_2 in the atmosphere continues to rise globally, endangering human health and the global ecosystem. Consequently, the development of materials and technologies for CO_2 capture and utilization is crucial for addressing the intractable global problem [1]. Numerous scientists and researchers have focused on the development of functional porous materials to capture and transform CO_2 under mild conditions [2], including zeolite [3,4], porous carbon [5,6], and metal-organic framework [7–9] among others. Porous organic polymers (POPs), as a class of emerging porous materials, are gradually attracting more research efforts due to their excellent physical and chemical stability, large surface area, good designability, and diverse structures, resulting in their wide applications in gas sorption [10–12], heterogeneous catalysis [13–15], sensor [16–18], and drug delivery [19–21]. Friedel-Crafts alkylation [22,23], Yamamoto reaction [24,25], Suzuki coupling reaction [26,27], and Sonogashira-Hagihara cross-coupling reaction [28,29] are examples of effective synthetic techniques that have been utilized to create POPs. However, some polymerization techniques have disadvantages that limit their applications in the synthesis of POPs, such as undesirable by-products, high energy consumption, low yield, harsh reaction conditions, and costly catalysts. Among these techniques, oxidative coupling polymerization utilizing $FeCl_3$ is regarded as one of the most popular approaches to constructing POF due to its low-cost, large-scale preparation, simple operation, and high universality [30–33]. On the other hand, carbazole and its derivatives are used as organic monomers to prepare POPs via $FeCl_3$-promoted oxidative coupling polymerization due to the large-conjugated system, rigid structure, high reactivity, and excellent photoelectric properties of carbazole and its

derivatives. Thus, some carbazole-based POPs have been synthesized and implemented in diverse fields [34–36].

In recent years, effective regulation of the interaction between CO_2 and porous skeletons has become an important area of research, as it is believed to be an energy-saving, accessible, and environmentally-friendly method for capturing and utilizing CO_2. By altering the skeleton configuration, stimuli-responsive porous materials are an effective way to regulate CO_2 sorption. Some porous functional materials have response properties to various external stimuli, including pH value [37], temperature [38], and light [39]. Light is a readily available source of renewable energy on Earth, and the introduction of light-responsive groups can alter the structures of porous materials [40]. Recently, metal-organic frameworks (MOFs) as a class of porous organic-inorganic hybrid materials have been utilized in a variety of applications [41–43], particularly photoresponsive MOFs for CO_2 sorption [44,45]. However, MOFs' poor stability severely restricts their application. POPs are more stable than MOFs and thus provide an excellent platform for light-responsive CO_2 capture. For high-performance CO_2 sorption, photoresponsive functional groups are the most important factor in the construction of POPs. Azobenzene is considered one of the readily available and light-sensitive groups. To date, azobenzene-functionalized light-responsive POPs with good photocontrol performance have attracted considerable interest in CO_2 capture [46,47]. Due to the exceptional photoelectric properties of carbazole and light-responsive azobenzene, carbazole-based POPs with azobenzene fragments serve as a platform for realizing light-responsive CO_2 sorption.

Based on our previous reports [48,49], we design and develop a carbazole-based azo-functionalized POP (JJU-2) by coupling 1,3,5-tris(9H-carbazole-9-yl) benzene (TCB) and azobenzene (AB) (Scheme 1). High stability, a large surface area, and well-developed pores characterize the prepared sample. In the meantime, the porous skeleton contains azo functional groups as a light-responsive sensitive component, resulting in stimuli-responsive CO_2 sorption through cis and trans structure transformations under ultraviolet (UV) irradiation and heat treatments. Furthermore, the controlled CO_2 sorption/release can be recycled at least three times without difficulty.

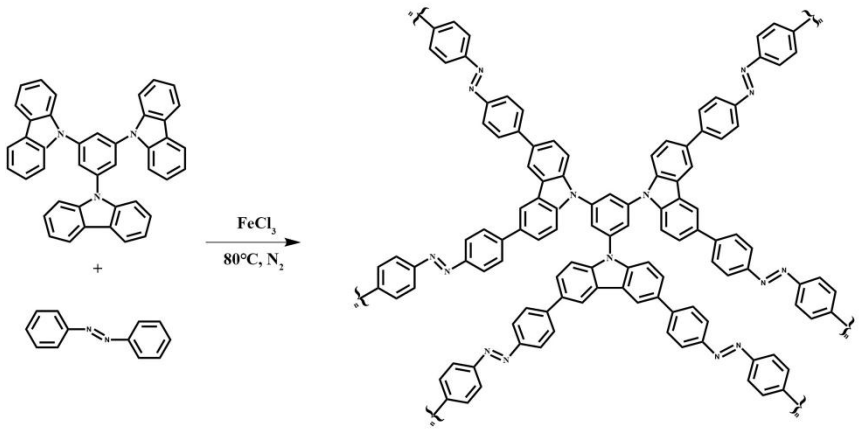

Scheme 1. The synthetic process of JJU-2.

2. Materials and Methods

2.1. Materials and General Methods

Unpurified chemicals were purchased and utilized. UV-Vis spectroscopy was carried out using a Mapada V-1200 (Shanghai Meipuda Instrument Co., Ltd., Shanghai, China). Using ZF-1A ultraviolet analyzer, trans-cis transformations were carried out (JIAPENG, Shanghai, China). IFS 66V/S Fourier transform infrared spectrometer was utilized to collect FT-IR spectra (Bruker Corporation, Rheinstetten, Germany). The ^{13}C solid NMR spectrum is performed on a Bruker AV-400-WB instrument (Bruker Corporation, Bill Erica, MA, USA). Rigaku D/MAX 2550 diffractometer records PXRD patterns (Rigaku, Tokyo, Japan)

with Cu-Kα (λ = 1.5418 Å) at 50 kV, 200 mA with a 2θ range of 4–40° at room temperature. The SEM images were acquired utilizing a MIRA-3 LMU scanning electron microscope (Tescan, Brno, Czech Republic). tecnai G2F20 S-TWIN was used to collect the TEM image (FEI, Hillsboro, WA, USA). The TGA curve was assessed using a PerkinElmer STA6000 thermal analyzer (PERKINELMER, Waltham, MA, USA) in the air. Gas sorptions were performed on Micromeritics before 2020 (Micromeritics Instrument Corporation, Norcross, GA, USA).

2.2. Synthesis of JJU-2

In a 100 mL round-bottom flask, 1,3,5-tris(9H-carbazole-9-yl) benzene (229 mg, 0.4 mmol, 1 eq), azobenzene (583 mg, 3.2 mmol, 8 eq), and $FeCl_3$ (583 mg, 3.6 mmol, 9 eq) were added, followed by three cycles of vacuuming and inserting with N_2. Then, 20 mL of dried $CHCl_3$ was added to the reaction system using a syringe. The reaction was heated at 80 °C for 24 h in an N_2 atmosphere. After the mixture cooled to room temperature, it was filtered to obtain the crude product. The product was further washed with HCl (0.3 M) aqueous solution, distilled water, methanol, and dichloromethane in order to remove unreacted monomers and catalyst residues. The product was dried under vacuum for 6 h at 60 °C to produce JJU-2 (orange solid powder, 463 mg, yield of 57%).

3. Results

3.1. Structural Description

The UV-visible adsorption spectra of azobenzene in dichloromethane exhibit a typical trans and cis isomerization transformation with obvious $\pi \rightarrow \pi^*$ absorption peaks, such as a strong peak at 319 nm and a weak peak at 435 nm (Figure 1a). To examine the successful polymerization of organic monomers and the structure of POPs, Fourier transform infrared (FT-IR) spectra are measured (Figure 1b). By comparing the FT-IR spectra of the initial monomers and JJU-2, the characteristic absorption peaks are summarized as follows: (a) there is an obvious absorption peak at 3000 cm^{-1}, which is mainly attributed to the C–H stretching vibration of the hydrogen atom in phenyl ring; (b) the C–H deformation vibration peaks (760–660 cm^{-1}) of four adjacent hydrogen atoms on the carbazolyl 1, 2-diXsubstituted phenyl ring is obviously weakened because the number of adjacent hydrogen atoms decreases from four to three; (c) some peaks in the range of 800–690 cm^{-1} belong to the C–H deformation vibration of ring hydrogen atoms of the 1,2-disubstituted phenyl ring of the carbazole group; (d) the peaks around 1300 cm^{-1} corresponds to the –C–N–bond between the aromatic ring and the azobenzene group; (e) FTIR bands located at 1458 cm^{-1} belongs to -N=N- stretching vibration in the azo-functional group in JJU-2, which confirms the successful synthesis of azo-linked POPs [50]. The ^{13}C solid-state NMR measurement is then used to examine the structure of the POP of interest (Figure 1c). Due to the presence of aromatic carbon atoms in the benzene ring, the ^{13}C solid-state NMR spectrum of JJU-2 exhibits three main peaks between 100 and 150 ppm. Notably, a high peak is observed at 123 ppm, which is attributable to unsubstituted phenyl carbon atoms, whereas two weak signals at 108 and 139 ppm are primarily attributable to substituted phenyl carbon atoms [51]. It further verifies the preparation of the JJU-2 target. As shown in Figure 1d, the thermogravimetric analysis (TGA) curve was measured in air at a heating rate of 10 °C min^{-1}. The first weight loss of the as-synthesized JJU-2 is about ~3.1% before ~330 °C, which may be attributed to the adsorbed water and other solvent molecules as the previous similar reports [52,53]. At higher temperatures, the skeleton gradually decomposes because of the oxygen reactions of C, N, and H elements in the air. The TGA curve confirms the good thermal stability of as-synthesized samples.

In addition, powder X-ray diffraction (PXRD) of as-synthesized POP reveals no diffraction peaks, indicating that as-synthesized JJU-2 is an amorphous solid material (Figure 2a). Using a scanning electron microscope (SEM) and transmission electron microscope (TEM), it is possible to observe the morphology and microstructure of JJU-2. The SEM image reveals that the prepared POP is an irregular crosslinked solid (Figure 2b). Moreover, the

TEM images of JJU-2 demonstrate that the synthesized POP has a disordered, worm-like porous structure (Figure 2c–e).

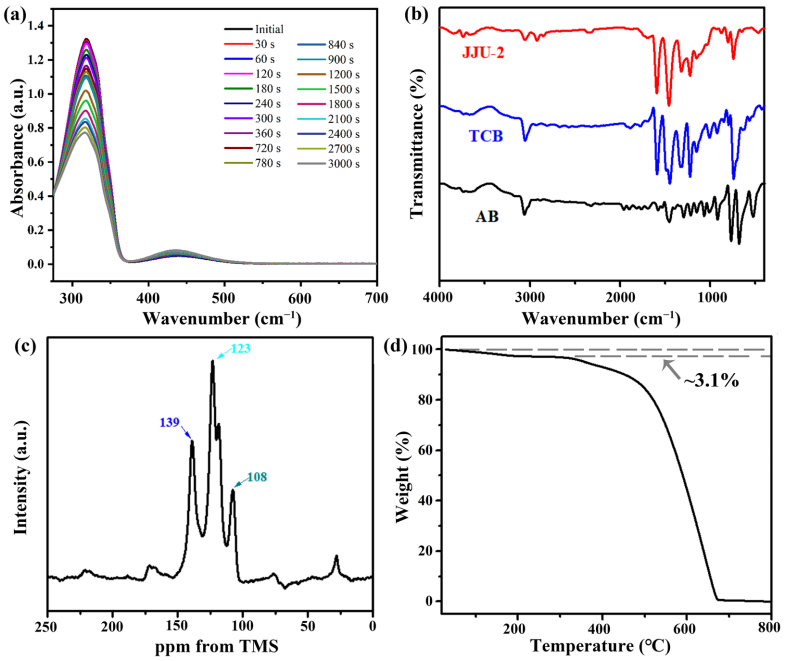

Figure 1. (**a**) UV-Vis adsorption spectra of azobenzene in dichloromethane under the irradiation with 365 nm light. (**b**) FT-IR of monomers and JJU-2; (**c**) ^{13}C solid-state NMR (cyan 123, blue 139, green 108); (**d**) TGA of JJU-2.

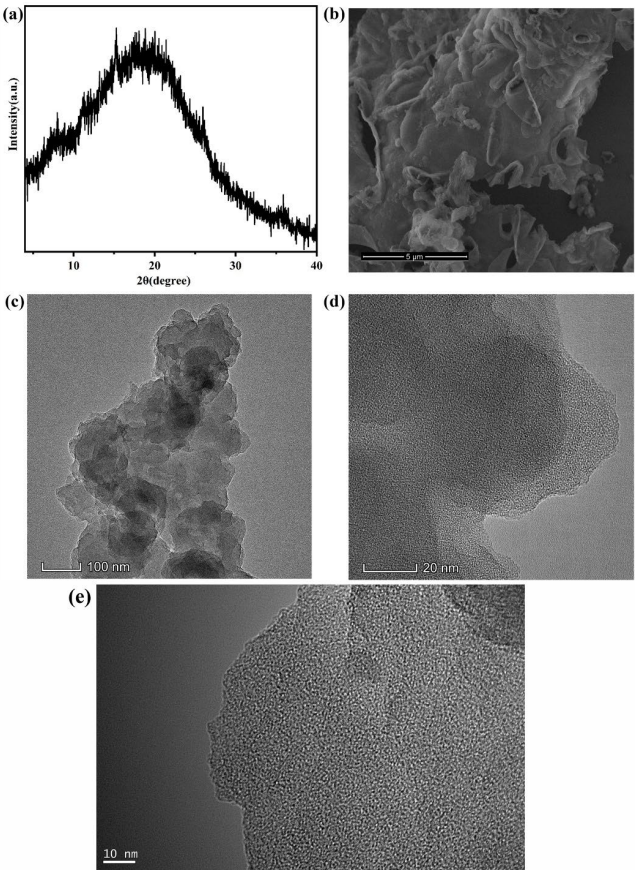

Figure 2. (**a**) PXRD, (**b**) SEM, and (**c**–**e**) TEM images of JJU-2.

3.2. Gas Sorption Properties

In order to examine the internal pores, synthesized JJU-2 is immersed in dichloromethane for two days and then activated at 150 °C for ten hours under a vacuum. The N_2 sorption isotherms of the initial sample were measured at 77 K, and after 5 h of UV irradiation, they were measured at 77 K once more. As depicted in Figure 3a, the majority of the curves exhibited a type I isotherm with a substantial capillary N_2 uptake in the low P/P_0 region. It confirms that JJU-1 is microporous. The desorption curves of both materials showed little hysteresis due to the diffusional limitation of adsorbed N_2 molecules in restricted micropores [54]. The sample surface areas are computed using the Langmuir and BET models, which are summarized in Table 1. Figure 3a and Table 2 demonstrate BET surface area plots. After 5 h of UV light irradiation, the surface area of the resultant material is smaller than that of the initial material. The NLDFT is utilized to determine the pore size distribution curves for both samples. After UV irradiation, the pore size distributions are between 0.50 nm and 1.27 nm, with a gradual decrease (Figure 3b). Similarly, the pore volumes of materials also undergo a change. Light-responsive azobenzene in the porous skeleton is primarily responsible for the pore change.

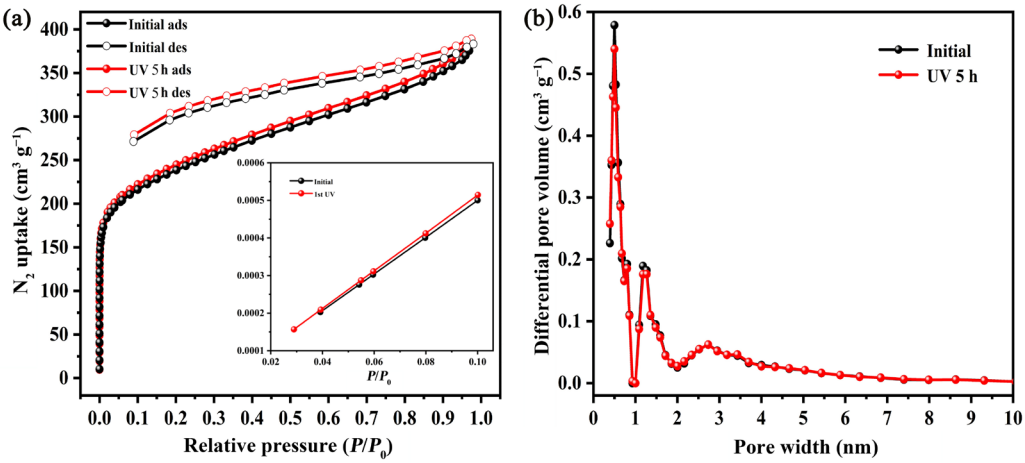

Figure 3. (**a**) N_2 adsorption and desorption isotherms of JJU-2 with the insert BET surface area plots, and (**b**) pore size distributions of JJU-2. Initial (black) and after UV irradiation for 5 h (red).

Table 1. Gas sorption properties for JJU-2.

POP Materials	SA_{BET} [a] [$m^2\ g^{-1}$]	$SA_{Langmuir}$ [b] [$m^2\ g^{-1}$]	Peak Pore Sizes [nm]	V_{Total} [c] [$cm^3\ g^{-1}$]	CO_2 Uptake [$cm^3\ g^{-1}$]		Q_{st} CO_2 [$kJ\ mol^{-1}$]
					273 K	298 K	
Initial	888.1	1002.7	0.27, 1.5	0.60	68.7	37.1	29.0
UV 5 h	864.6	976.3	0.27, 1.5	0.59	63.2	34.4	26.5

Surface areas calculated from BET [a] and Langmuir [b] models; [c] The total pore volume calculated at $P/P_0 = 0.97$.

Table 2. BET surface areas of JJU-2.

POP Materials	BET [$m^2\ g^{-1}$]	Slope [$g\ cm^{-3}$]	*Y*-Intercept [$g\ cm^{-3}$]	*C*	Q_m [$cm^3\ g^{-1}$]	Correlation Coefficient
Initial	888.1	0.004890	0.000011	450.072216	204.0409	0.999997
UV 5 h	864.6	0.005023	0.000011	439.286920	198.6445	0.999998

Based on previous research, the trans/cis isomerization of azobenzene can result in different geometric and dipole variations [55–57]. The dynamic structural changes of

as-synthesized POP can be used as a light-responsive CO_2 adsorbent under mild conditions; therefore, the CO_2 sorption isotherms are carried out at 273 and 298 K, respectively, under 1 atmosphere. The initial POP has a strong capacity for CO_2 sorption, with a maximum absorption of 68 cm^3 g^{-1} at 273 K and 37 cm^3 g^{-1} at 298 K and 1 atm (Figure 4a). Notably, after 5 h of UV irradiation, JJU-2 exhibits different CO_2 sorption behaviors due to the trans/cis isomerization of azobenzene in its porous structure. As shown in Figure 4b, the CO_2 sorption amount decreases to 62 cm^3 g^{-1} at 273 K and 34 cm^3 g^{-1} at 298 K. Similar to the previous reports [58–60], the hysteresis of the CO_2 desorption is mainly ascribed to the electronic attraction between adsorbed and desorbed CO_2 molecules, and the interaction between the porous skeleton and CO_2. Meanwhile, it is probably caused by the pore window and pore expansion in POPs.

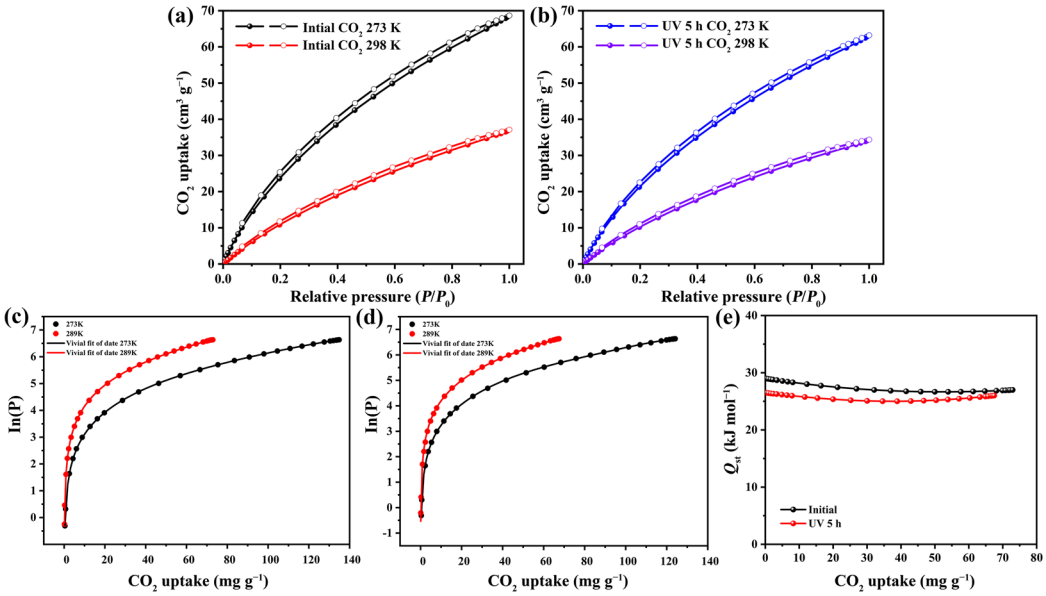

Figure 4. CO_2 adsorption isotherms of (**a**) initial JJU-2 and (**b**) JJU-2 after UV irradiation for 5 h; the fitting data for calculating the CO_2 Q_{st} value for (**c**) JJU-2-initial and (**d**) JJU-2-1st UV; (**e**) the calculated Q_{st} plots.

Using CO_2 adsorption at 273 and 298 K, the CO_2 adsorption enthalpy (Qst) can be calculated to determine the interaction force between CO_2 and the skeleton of JJU-2 (Figure 4c,d). The calculated CO_2 Q_{st} value of the initial sample is as high as 29.0 kJ mol^{-1}, but after 5 h of UV irradiation, the value decreases to 26.5 kJ mol^{-1}, proving the trans/cis structure transformation of JJU-2 (Figure 4e). Table 3 provides samples of representative materials [48,49,61–70].

According to the porous structure of initial and UV-treated samples, the decreased micropore volume may be the main reason for reducing the CO_2 adsorption capacity of JJU-2 after irradiating by UV light. Reversible circularity is another vital factor for stimulus-responsive CO_2 sorption porous materials. As illustrated in Figure 5a–e and Table 4, the CO_2 adsorption isotherms of JJU-2 are repeatedly measured for three cycles after UV irradiation and thermal regeneration, which exhibits that the as-synthesized JJU-2 has good light- and thermal-responsive circularity for adsorbing CO_2 at 273 K under 1 atm under the controllable external stimulation.

Table 3. Summary of CO_2 uptake and Q_{st} value for some reported porous materials.

Materials	BET [$m^2\ g^{-1}$]	V_{Total} [$cm^3\ g^{-1}$]	CO_2 Uptake ($cm^3\ g^{-1}$) (273 K, 1 Bar)	Q_{st} CO_2 (kJ mol^{-1})	Ref.
JJU-1	467	0.31	45.3	27.1	[48]
JJU-1-UV	469	0.34	40.1	33.1	[48]
POF-Initial	571	0.49	46.2	26.7	[49]
POF-1stUV	549	0.48	41.6	29.7	[49]
Azo-MOP-1	456	0.48	49.6	-	[61]
PAF-36	325	0.25	28.6	27.0	[62]
PAF-36-UV	385	0.27	31.2	28.4	[62]
PAF-37	443	0.27	26.3	36.8	[62]
PAF-37-UV	456	0.28	29.6	40.7	[62]
TAP-1	474	0.74	48.4	35.6	[63]
azo-COP-1	608	0.39	54.7	29.3	[64]
azo-COP-2	703	0.42	56.2	24.8	[64]
Azo-POF-1	712	-	66.7	27.5	[65]
Azo-POF-2	439	-	43.0	26.6	[65]
ALP-4	862	0.50	41.2	28.2	[66]
PCN-250-Fe_3 (II/III)	1619	-	133.66	-	[67]
PCN-250-Fe_3 (III)	1598	-	50.81	-	[67]
PCN-250-Al_3	1874	-	170.48	-	[67]
PCN-250-Sc_3	1321	-	101.31	-	[67]
PCN-250-In_3	1224	-	108.15	-	[67]
MS	1015	0.96	-	-	[68]
DAL(1)@MS	627	0.46	-	-	[68]
DAL(2)@MS	589	0.40	50	-	[68]
DAL(2)@MS UV	-	-	33	-	[68]
DAL(3)@MS	512	0.31	-	-	[68]
BCzMB@PON	865	-	90.048	31.96	[69]
TPA@PON	829	-	86.24	37.98	[69]
CZ@PON	592	-	96.544	42.01	[69]
HMC-1	855	0.2968	235.2 (273 K, 3 bar)	-	[70]
HMC-2	425	0.1920	306.88 (273 K, 3 bar)	-	[70]
HMC-3	526	0.1618	318.08 (273 K, 3 bar)	-	[70]
JJU-2	888.1	0.60	68.7	29.0	This Work
JJU-2-UV	864.6	0.59	63.2	26.5	This Work

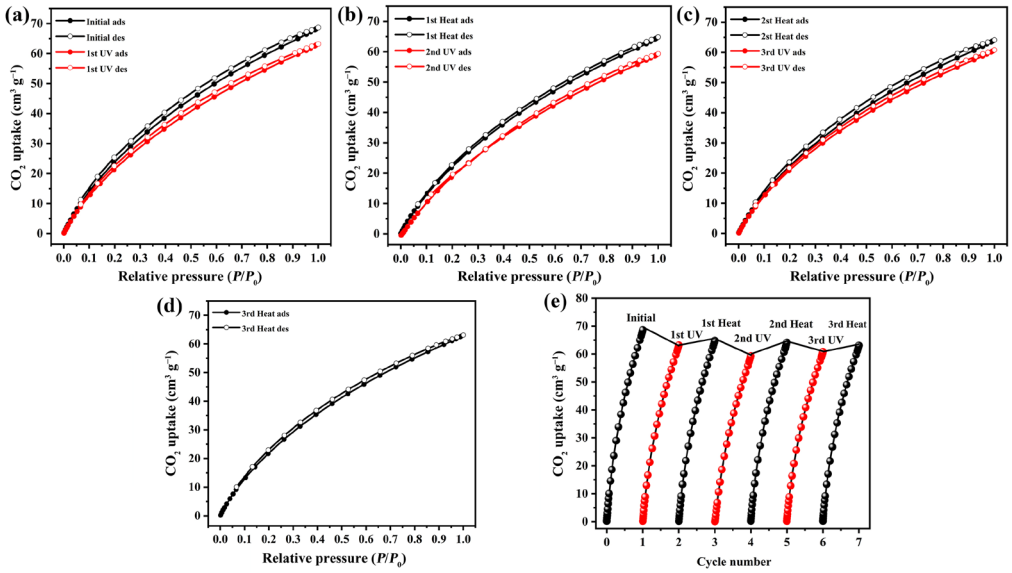

Figure 5. (**a**–**d**) The CO_2 adsorption isotherms of initial JJU-2 and JJU-2 after UV irradiation for 3 cycles; (**d**) the cyclic responsiveness of JJU-2 after UV irradiation and heat treatments; (**e**) the reversibility of JJU-2 after UV and heat treatment for three cycles.

Table 4. The CO_2 maximum adsorption amounts for JJU-2 at 273 K and 1 bar.

JJU-2	CO_2 Uptake [cm^3 g^{-1}]
Initial	68.7
1st UV	63.2
1st Heat	64.8
2nd UV	59.3
2nd Heat	64.1
3rd UV	60.8
3rd Heat	63.1

4. Conclusions

In conclusion, an Azo-Functionalized POP is designed and synthesized via an oxidative coupling method. The porous structure and light-responsive properties of this POP material are investigated in depth. In POPs, UV irradiation and thermal regeneration can specifically affect the trans/cis transition of azo groups. Under UV irradiation, the capacity for CO_2 sorption decreases by 8%. In the meantime, this stimuli-responsive POP can revert to its original structure following thermal regeneration. According to recycling tests, the CO_2 adsorption performance of this synthesized POP can be recycled at least three times via UV irradiation and thermal regeneration. This study aims to provide a method for constructing POPs with CO_2 adsorption that are reversibly stimulated.

Author Contributions: Writing—original draft preparation, R.Y. and M.Z.; methodology, H.S. All authors have read and agreed to the published version of the manuscript.

Funding: This research was funded by the financial support of National Natural Science Foundation of China (21805109).

Institutional Review Board Statement: Not applicable.

Data Availability Statement: No new data were created or analyzed in this study. Data sharing is not applicable to this article.

Conflicts of Interest: The authors declare no conflict of interest.

References

1. Zhang, Z.; Wang, T.; Blunt, M.J.; Anthony, E.J.; Park, A.A.; Hughes, R.W.; Webley, P.A.; Yan, J. Advances in carbon capture, utilization and storage. *Appl. Energy* **2020**, *278*, 115627. [CrossRef]
2. Ding, M.; Liu, X.; Ma, P.; Yao, J. Porous materials for capture and catalytic conversion of CO_2 at low concentration. *Coordin. Chem. Rev.* **2022**, *465*, 214576. [CrossRef]
3. Liu, J.; Zhang, Z.; Jiang, Y.; Jiang, X.; He, N.; Yan, S.; Guo, P.; Xiong, G.; Su, J.; Vile, G. Influence of the zeolite surface properties and potassium modification on the Zn-catalyzed CO_2-assisted oxidative dehydrogenation of ethane. *Appl. Catal. B-Environ.* **2022**, *304*, 120947. [CrossRef]
4. Bikbaeva, V.; Nesterenko, N.; Konnov, S.; Nguyen, T.S.; Gilson, J.P.; Valtchev, V. A low carbon route to ethylene: Ethane oxidative dehydrogenation with CO_2 on embryonic zeolite supported Mo-carbide catalyst. *Appl. Catal. B-Environ.* **2023**, *320*, 122011. [CrossRef]
5. Shen, Y. Preparation of renewable porous carbons for CO_2 capture–A review. *Fuel Process. Technol.* **2022**, *236*, 107437. [CrossRef]
6. Yu, A.; Ma, G.; Zhu, L.; Zhang, R.; Li, Y.; Yang, S.; Hsu, H.Y.; Peng, P.; Li, F.F. Conversion of CO_2 to defective porous carbons in one electro-redox cycle for boosting electrocatalytic H_2O_2 production. *Appl. Catal. B-Environ.* **2022**, *307*, 121161. [CrossRef]
7. He, H.; Sun, Q.; Gao, W.; Perman, J.A.; Sun, F.; Zhu, G.; Aguila, B.; Forrest, K.; Space, B.; Ma, S. A stable metal-organic framework featuring a local buffer environment for carbon dioxide fixation. *Angew. Chem. Int. Edit.* **2018**, *57*, 4657–4662. [CrossRef]
8. Gulati, S.; Vijayan, S.; Kumar, S.; Harikumar, B.; Trivedi, M.; Varma, R.S.; Varma, R.S. Recent advances in the application of metal-organic frameworks (MOFs)-based nanocatalysts for direct conversion of carbon dioxide (CO_2) to value-added chemicals. *Coordin. Chem. Rev.* **2023**, *474*, 214853. [CrossRef]
9. Mallakpour, S.; Nikkhoo, E.; Hussain, C.M. Application of MOF materials as drug delivery systems for cancer therapy and dermal treatment. *Coordin. Chem. Rev.* **2022**, *451*, 214262. [CrossRef]
10. Panić, B.; Frey, T.; Borovina, M.; Konopka, K.; Sambolec, M.; Kodrin, I.; Biljan, I. Synthesis and characterization of benzene- and triazine-based azo-bridged porous organic polymers. *Polymers* **2023**, *15*, 229. [CrossRef]
11. Zhou, H.; Rayer, C.; Antonangelo, A.R.; Hawkins, N.; Carta, M. Adjustable functionalization of hyper-cross-linked polymers of intrinsic microporosity for enhanced CO_2 adsorption and selectivity over N_2 and CH_4. *ACS Appl. Mater. Interfaces* **2022**, *14*, 20997–21006. [CrossRef]
12. Zhao, X.; Qi, Y.; Li, J.; Ma, Q. Porous organic polymers derived from ferrocene and tetrahedral silicon-centered monomers for carbon dioxide sorption. *Polymers* **2022**, *14*, 370. [CrossRef] [PubMed]
13. Henrion, M.; Mohr, Y.; Janssens, K.; Smolders, S.; Bugaev, A.L.; Usoltsev, O.A.; Quadrelli, E.A.; Wisser, F.M.; De Vos, D.E.; Canivet, J. Reusable copper catechol-based porous polymers for the highly efficient heterogeneous catalytic oxidation of secondary alcohols. *ChemCatChem* **2022**, *14*, e202200649. [CrossRef]
14. Saber, A.F.; Elewa, A.M.; Chou, H.H.; EL-Mahdy, A.F.M. Donor-acceptor carbazole-based conjugated microporous polymers as photocatalysts for visible-light-driven H_2 and O_2 evolution from water splitting. *Appl. Catal. B-Environ.* **2022**, *316*, 121624. [CrossRef]
15. Dong, X.; Hao, H.; Zhang, F.; Lang, X. Blue light photocatalysis of carbazole-based conjugated microporous polymers: Aerobic hydroxylation of phenylboronic acids to phenols. *Appl. Catal. B-Environ.* **2022**, *309*, 121210. [CrossRef]
16. Yuan, R.; Yan, Z.; Shaga, A.; He, H. Design and fabrication of an electrochemical sensing platform based on a porous organic polymer for ultrasensitive ampicillin detection. *Sens. Actuat. B Chem.* **2021**, *327*, 128949. [CrossRef]
17. Zhang, Y.X. The preparation of 2,2′-bithiophene-based conjugated microporous polymers by direct arylation polymerization and their application in fluorescence sensing 2,4-dinitrophenol. *Anal. Chim. Acta* **2023**, *1240*, 340779. [CrossRef]
18. Han, Z.Y.; Li, H.K.; Zhu, Q.Q.; Yuan, R.R.; He, H. An intriguing electrochemical impedance aptasensor based on a porous organic framework supported silver nanoparticles for ultrasensitively detecting theophylline. *Chin. Chem. Lett.* **2021**, *32*, 2865–2868. [CrossRef]
19. Jiang, X.; Wang, Q.; Liu, Y.; Fu, X.; Luo, Y.; Lyu, Y. A nanoscale porous glucose-based polymer for gas adsorption and drug delivery. *New J. Chem.* **2018**, *42*, 15692–15697. [CrossRef]
20. Zhang, H.; Li, G.; Liao, C.; Cai, Y.; Jiang, G. Bio-related applications of porous organic frameworks (POFs). *J. Mater. Chem. B* **2019**, *7*, 2398–2420. [CrossRef]
21. Singh, N.; Son, S.; An, J.; Kim, I.; Choi, M.; Kong, N.; Tao, W.; Kim, J.S. Nanoscale porous organic polymers for drug delivery and advanced cancer theranostics. *Chem. Soc. Rev.* **2021**, *50*, 12883–12896. [CrossRef] [PubMed]
22. Troschke, E.; Graetz, S.; Luebken, T.; Borchardt, L. Mechanochemical Friedel-Crafts alkylation-A sustainable pathway towards porous organic polymers. *Angew. Chem. Int. Edit.* **2017**, *56*, 6859–6863. [CrossRef]
23. Hao, S.; Liu, Y.; Shang, C.; Liang, Z.; Yu, J. CO_2 adsorption and catalytic application of imidazole ionic liquid functionalized porous organic polymers. *Polym. Chem.* **2017**, *8*, 1833–1839. [CrossRef]
24. Guo, L.; Cao, D. Color tunable porous organic polymer luminescent probes for selective sensing of metal ions and nitroaromatic explosives. *J. Mater. Chem. C* **2015**, *3*, 8490–8494. [CrossRef]
25. Fischer, S.; Schimanowitz, A.; Dawson, R.; Senkovska, I.; Kaskel, S.; Thomas, A. Cationic microporous polymer networks by polymerisation of weakly coordinating cations with CO_2-storage ability. *J. Mater. Chem. A* **2014**, *2*, 11825–11829. [CrossRef]
26. Yan, Z.; Qiao, Y.; Wang, J.; Xie, J.; Cui, B.; Fu, Y.; Lu, J.; Yang, Y.; Bu, N.; Yuan, Y.; et al. An azo-group-functionalized porous aromatic framework for achieving highly efficient capture of iodine. *Molecules* **2022**, *27*, 6297. [CrossRef]

27. Yan, Z.; Liu, J.; Miao, C.; Su, P.; Zheng, G.; Cui, B.; Geng, T.; Fan, J.; Yu, Z.; Bu, N.; et al. Pyrene-based fluorescent porous organic polymers for recognition and detection of pesticides. *Molecules* **2022**, *27*, 126. [CrossRef]
28. Yuan, R.; Liu, Z.; Sun, H.; He, H. Porphyrin-based porous organic frameworks for the ultrasensitive electrochemical impedimetric aptasensing of oxytetracycline. *Appl. Surf. Sci.* **2021**, *569*, 151038. [CrossRef]
29. Bildirir, H.; Paraknowitsch, J.P.; Thomas, A. A tetrathiafulvalene (TTF)-conjugated microporous polymer network. *Chem.-Eur. J.* **2014**, *20*, 9543–9548. [CrossRef]
30. Yuan, R.; He, H. Construction of an electrochemical aptasensor based on a carbazole-bearing porous organic polymer for rapid and ultrasensitive detection of penicillin. *Appl. Surf. Sci.* **2021**, *563*, 150307. [CrossRef]
31. Mohamed, M.G.; EL-Mahdy, A.F.M.; Meng, T.S.; Samy, M.M.; Kuo, S.W. Multifunctional hypercrosslinked porous organic polymers based on tetraphenylethene and triphenylamine derivatives for high-performance dye adsorption and supercapacitor. *Polymers* **2020**, *12*, 2426. [CrossRef]
32. Wang, D.G.; Song, F.; Tang, H.; Jia, X.R.; Song, M.; Kuang, G.C. A facile route to prepare dimeric BODIPY-based porous organic polymers using $FeCl_3$. *New J. Chem.* **2017**, *41*, 5263–5266. [CrossRef]
33. Schute, K.; Rose, M. Metal-free and scalable synthesis of porous hyper-cross-linked polymers: Towards applications in liquid-phase adsorption. *ChemSusChem* **2015**, *8*, 3419–3423. [CrossRef]
34. Xu, Y.; Yu, H.; Shi, B.; Gao, S.; Zhang, L.; Li, X.; Liao, X.; Huang, K. Room-temperature synthesis of hollow carbazole-based covalent triazine polymers with multiactive sites for efficient iodine capture-catalysis cascade application. *ACS Appl. Polym. Mater.* **2020**, *2*, 3704–3713. [CrossRef]
35. Qian, L.; Hong, H.; Han, M.; Xu, C.; Wang, S.; Guo, Z.; Yan, D. A ketone-functionalized carbazolic porous organic framework for sensitive fluorometric determination of p-nitroaniline. *Microhim. Acta* **2019**, *186*, 457. [CrossRef] [PubMed]
36. Liu, C.; Li, Y.; Zhang, M.; Yuan, K.; Liang, S.; Yu, G.; Weng, Z.; Jian, X. Hierarchical porous organic hyper-cross-linked polymers containing phthalazinone and carbazole moieties for gas uptake and fluorescence properties. *Eur. Polym. J.* **2020**, *130*, 109674. [CrossRef]
37. Wang, H.; Zhu, W.; Liu, J.; Dong, Z.; Liu, Z. pH-Responsive nanoscale covalent organic polymers as a biodegradable drug carrier for combined photodynamic chemotherapy of cancer. *ACS Appl. Mater. Interfaces* **2018**, *10*, 14475–14482. [CrossRef]
38. Comotti, A.; Bracco, S.; Ben, T.; Qiu, S.; Sozzani, P. Molecular rotors in porous organic frameworks. *Angew. Chem. Int. Edit.* **2014**, *53*, 1043–1047. [CrossRef] [PubMed]
39. Xue, D.M.; Zhang, W.J.; Liu, X.Q.; Qi, S.C.; Sun, L.B. Fabrication of azobenzene-functionalized porous polymers for selective CO_2 capture. *Chin. J. Chem. Eng.* **2022**, *43*, 24–30. [CrossRef]
40. Danowski, W.; van Leeuwen, T.; Browne, W.R.; Feringa, B.L. Photoresponsive porous materials. *Nanoscale Adv.* **2021**, *3*, 24–40. [CrossRef] [PubMed]
41. Tao, C.A.; Li, Y.; Wang, J. The progress of electrochromic materials based on metal-organic frameworks. *Coordin. Chem. Rev.* **2023**, *475*, 214891. [CrossRef]
42. He, H.; Wen, H.-M.; Li, H.-K.; Zhang, H.-W. Recent advances in metal-organic frameworks and their derivatives for electrocatalytic nitrogen reduction to ammonia. *Coordin. Chem. Rev.* **2022**, *471*, 214761. [CrossRef]
43. Adegoke, K.A.; Adegoke, O.R.; Adigun, R.A.; Maxakata, N.W.; Bello, O.S. Two-dimensional metal-organic frameworks: From synthesis to biomedical, environmental, and energy conversion applications. *Coordin. Chem. Rev.* **2022**, *473*, 214817. [CrossRef]
44. Huang, Q.; Mu, J.; Zhan, Z.; Wang, F.; Jin, S.; Tan, B.; Wu, C. A steric hindrance alleviation strategy to enhance the photo-switching efficiency of azobenzene functionalized metal-organic frameworks toward tailorable carbon dioxide capture. *J. Mater. Chem. A* **2022**, *10*, 8303–8308. [CrossRef]
45. Zhang, X.; Yu, T.; Au, V.K.M. Photoresponsive metal-organic frameworks: Tailorable platforms of photoswitches for advanced functions. *ChemNanoMat* **2022**, *8*, e202100486. [CrossRef]
46. Baroncini, M.; d'Agostino, S.; Bergamini, G.; Ceroni, P.; Comotti, A.; Sozzani, P.; Bassanetti, I.; Grepioni, F.; Hernandez, T.M.; Silvi, S.; et al. Photoinduced reversible switching of porosity in molecular crystals based on star-shaped azobenzene tetramers. *Nat. Chem.* **2015**, *7*, 634–640. [CrossRef] [PubMed]
47. Zhu, Y.; Zhang, W. Reversible tuning of pore size and CO_2 adsorption in azobenzene functionalized porous organic polymers. *Chem. Sci.* **2014**, *5*, 4957–4961. [CrossRef]
48. Yuan, R.; Sun, H.; He, H. Rational construction of a responsive azo-functionalized porous organic framework for CO_2 sorption. *Molecules* **2021**, *26*, 4993. [CrossRef]
49. Yuan, R.; Sun, H.; Yan, Z.; He, H. Rational design and synthesis of a task-specific porous organic framework featured azobenzene as a photoresponsive low-energy CO_2 adsorbent. *J. Solid State Chem.* **2021**, *297*, 122049. [CrossRef]
50. Li, S.; Prasetya, N.; Ladewig, B.P. Investigation of azo-COP-2 as a photoresponsive low-energy CO_2 adsorbent and porous filler in mixed matrix membranes for CO_2/N_2 separation. *Ind. Eng. Chem. Res.* **2019**, *58*, 9959–9969. [CrossRef]
51. Yuan, R.; Yan, Z.; Shaga, A.; He, H. Solvent-free mechanochemical synthesis of a carbazole-based porous organic polymer with high CO_2 capture and separation. *J. Solid State Chem.* **2020**, *287*, 121327. [CrossRef]
52. Nie, W.; Liu, J.; Bai, X.; Xing, Z.; Gao, Y. Designing phenyl porous organic polymers with high-efficiency tetracycline adsorption capacity and wide pH adaptability. *Polymers.* **2022**, *14*, 203. [CrossRef] [PubMed]
53. Geng, T.; Zhang, W.; Zhu, Z.; Chen, G.; Ma, L.; Ye, S.; Niu, Q. A covalent triazine-based framework from tetraphenylthiophene and 2,4,6-trichloro-1,3,5-triazine motifs for sensing o-nitrophenol and effective I_2 uptake. *Polym. Chem.* **2018**, *9*, 777–784. [CrossRef]

54. Ruidas, S.; Das, A.; Kumar, S.; Dalapati, S.; Manna, U.; Bhaumik, A. Non-fluorinated and robust superhydrophobic modification on covalent organic framework for crud-oil-in-water emulsion separation. *Angew. Chem. Int. Ed.* **2022**, *61*, e202210507. [CrossRef] [PubMed]
55. Kanj, A.B.; Mueller, K.; Heinke, L. Stimuli-responsive metal–organic frameworks with photoswitchable azobenzene side groups. *Macromol. Rapid Commun.* **2018**, *39*, 1700239. [CrossRef] [PubMed]
56. Bujak, K.; Nocon, K.; Jankowski, A.; Wolinska-Grabczyk, A.; Schab-Balcerzak, E.; Janeczek, H.; Konieczkowska, J. Azopolymers with imide structures as light-switchable membranes in controlled gas separation. *Eur. Polym. J.* **2019**, *118*, 186–194. [CrossRef]
57. Mukhopadhyay, R.D.; Praveen, V.K.; Ajayaghosh, A. Photoresponsive metal–organic materials: Exploiting the azobenzene switch. *Mater. Horiz.* **2014**, *1*, 572–576. [CrossRef]
58. Song, K.S.; Fritz, P.W.; Coskun, A. Porous organic polymers for CO_2 capture, separation and conversion. *Chem. Soc. Rev.* **2022**, *51*, 9831–9852. [CrossRef] [PubMed]
59. Bhanja, P.; Modak, A.; Bhaumik, A. Porous organic polymers for CO_2 storage and conversion reactions. *ChemCatChem* **2019**, *11*, 244–257. [CrossRef]
60. Dai, Z.; Long, Y.; Liu, J.; Bao, Y.; Zheng, L.; Ma, J.; Liu, J.; Zhang, F.; Xiong, Y.; Lu, J.Q. Functional porous ionic polymers as efficient heterogeneous catalysts for the chemical fixation of CO_2 under mild conditions. *Polymers* **2022**, *14*, 2658. [CrossRef]
61. Yang, Z.; Zhang, H.; Yu, B.; Zhao, Y.; Ma, Z.; Ji, G.; Han, B.; Liu, Z. Azo-functionalized microporous organic polymers: Synthesis and applications in CO_2 capture and conversion. *Chem. Commun.* **2015**, *51*, 11576–11579. [CrossRef]
62. Yuan, R.; Ren, H.; He, H.; Jiang, L.; Zhu, G. Targeted synthesis of porous aromatic frameworks with stimuli-responsive adsorption properties. *Sci. China Mater.* **2015**, *58*, 38–43. [CrossRef]
63. Bera, R.; Ansari, M.; Alam, A.; Das, N. Triptycene, phenolic-OH and azo-functionalized porous organic polymers: Efficient and selective CO_2 capture. *ACS Appl. Polym. Mater.* **2019**, *1*, 959–968. [CrossRef]
64. Patel, H.A.; Je, S.H.; Park, J.; Chen, D.P.; Jung, Y.; Yavuz, C.T.; Coskun, A. Unprecedented high-temperature CO_2 selectivity in N_2-phobic nanoporous covalent organic polymers. *Nat. Commun.* **2013**, *4*, 1357. [CrossRef]
65. Lu, J.; Zhang, J. Facile synthesis of azo-linked porous organic frameworks via reductive homocoupling for selective CO_2 capture. *J. Mater. Chem. A* **2014**, *2*, 13831–13834. [CrossRef]
66. Arab, P.; Rabbani, M.G.; Sekizkardes, A.K.; İslamoğlu, T.; El-Kaderi, H.M. Copper(I)-catalyzed synthesis of nanoporous azo-linked polymers: Impact of textural properties on gas storage and selective carbon dioxide capture. *Chem. Mater.* **2014**, *26*, 1385–1392. [CrossRef]
67. Drake, H.F.; Xiao, Z.; Day, G.S.; Vali, S.W.; Daemen, L.L.; Cheng, Y.; Cai, P.; Kuszynski, J.E.; Lin, H.; Zhou, H.C.; et al. Influence of metal identity on light-induced switchable adsorption in azobenzene-based metal-organic frameworks. *ACS Appl. Mater. Interfaces* **2022**, *14*, 11192–11199. [CrossRef]
68. Tan, P.; Jiang, Y.; Wu, Q.; Gu, C.; Qi, S.; Zhang, Q.; Liu, X.; Sun, L. Light-responsive adsorbents with tunable adsorbent–adsorbate interactions for selective CO_2 capture. *Chin. J. Chem. Eng.* **2022**, *42*, 104–111. [CrossRef]
69. Mondal, S.; Kundu, S.K.; Bhaumik, A.A. Facile approach for the synthesis of hydroxyl-rich microporous organic networks for efficient CO_2 capture and H_2 storage. *Chem. Commun.* **2017**, *53*, 2752–2755. [CrossRef] [PubMed]
70. Kundu, S.K.; Bhaumik, A. Novel nitrogen and sulfur rich hyper-cross-linked microporous poly-triazine-thiophene copolymer for superior CO_2 capture. *ACS Sustain. Chem. Eng.* **2016**, *4*, 3697–3703. [CrossRef]